Determination of the bubble-to-emulsion phase mass transfer coefficient in gas-solid fluidized beds using a non-invasive infra-red technique

Chemical Engineering Journal 325 (2017) 404–414

Contents lists available at ScienceDirect

Chemical Engineering Journal

journal homepage: www.elsevier.com/locate/cej

Determination of the bubble-to-emulsion phase mass transfer coefficient in gas-solid fluidized beds using a non-invasive infra-red technique

J.A. Medrano, F. Gallucci *, F. Boccia, N. Alfano, M. van Sint Annaland

Chemical Process Intensification, Department of Chemical Engineering and Chemistry, Eindhoven University of Technology, De Rondom 70, 5612 AP Eindhoven, The Netherlands

HIGHLIGHTS

- Non-intrusive IR technique used to investigate mass transfer in fluidized beds.
- Whole-field bubble reconstruction to visualize gas tracer concentration profiles.
- Mass transfer in isolated bubbles in good agreement with theoretical descriptions.
- Mass transfer is clearly enhanced in bubbling beds.

GRAPHICAL ABSTRACT

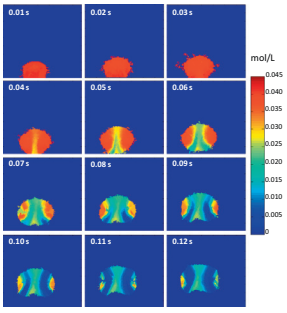

ARTICLE INFO

Article history:
Received 3 April 2017
Received in revised form 12 May 2017
Accepted 14 May 2017
Available online 16 May 2017

Keywords:
Mass transfer
Fluidized bed
Bubble injection
IR technique

ABSTRACT

The theoretical approach for the bubble-to-emulsion phase mass exchange in bubbling gas-solid fluidized beds developed by Davidson and Harrison in the early 60's is still widely applied in phenomenological models, mainly because of lack of more detailed experimental data to improve the description. In this study a novel infrared transmission technique that allows the direct and non-invasive measurement of gas concentration profiles inside bubbles with a high temporal resolution has been used for the validation of the theoretical description for the gas exchange. At first, the experimental technique has been further improved concerning the selective removal of particles raining through the bubbles, as well as the reconstruction of tracer gas concentration profiles throughout the gas bubble. The bubble-to-emulsion phase mass transfer coefficients have been measured by injecting tracer gas bubbles into incipiently fluidized beds and beds at freely-bubbling conditions, for beds consisting of glass beads of different particle size and with different injected bubble diameters. The results show that the Davidson and Harrison approach can reasonably well describe the mass exchange for isolated bubbles injected into a bed at minimum fluidization conditions. However, experiments carried out in a freely bubbling bed have shown that the mass exchange rate is considerably enhanced due to the increased gas through-flow through the bubbles. An empirical correlation (with deviations within only 20%) for the volumetric bubble-to-emulsion phase mass transfer coefficient has been developed based on the bubble size and superficial gas velocity, where it is noted that in this work the convective contribution in the mass exchange is dominant.

1. Introduction

For many different applications gas-solid fluidized beds are preferred over other contactors because of their excellent heat and

* Corresponding author.
E-mail address: f.gallucci@tue.nl (F. Gallucci).

http://dx.doi.org/10.1016/j.cej.2017.05.089
1385-8947/

Nomenclature

A	absorbance, –
C	gas concentration, mol/L
$C_{t,b}$, $C_{t,e}$	tracer gas concentration as function of time in the bubble and emulsion phases respectively, mol/L
d_b	bubble diameter, m
D_G	gas diffusion coefficient, m^2/s
ε	molar absorbance, $mol^{-1}\ cm^{-2}$
ε_{mf}	bed voidage at incipient fluidization conditions, –
f_w	fraction of the wake phase in a fluidized bed, –
g	gravitational constant, m/s^2
I	IR intensity, –
k_{bc}	gas exchange coefficient between the bubble and cloud phases, s^{-1}
k_{be}	gas exchange coefficient between the bubble and emulsion phases, s^{-1}
k_{ce}	gas exchange coefficient between the cloud and emulsion phases, s^{-1}
ℓ	target length, cm
T	transmittance, –
t	time, s
u_0	superficial gas velocity, m/s
u_b	bubble velocity, m/s
u_{mf}	superficial gas velocity at minimum fluidization conditions, m/s
V_b	bubble volume, m^3

mass transfer characteristics, and efficient particle and thermal mixing inside the reactor [1,2]. Fluidization can be defined as the operation where solid particles are suspended in a fluid rendering the solids phase a fluid-like behavior. When the flow rate of gas fed into the system is just sufficient to suspend the particulate phase (i.e. when the drag force equals the effective gravitational force), the system is at its minimum fluidization conditions, and excess of gas induces the formation of gas voids that rise and coalesce along the bed height. These gas bubbles are responsible of the excellent contacting and mixing of the gas and particles, as they cause macroscale solids circulation inside the reactor. The bubble properties and the movement of the solids are related to the hydrodynamics, while the contact between the gas and solid phases and, in particular, the exchange between the gas inside the bubbles and the gas in the emulsion phase is dictated by mass transfer.

The hydrodynamics in fluidized beds have been extensively studied in the literature using many different experimental techniques in 2D (i.e. with small column depth) and 3D reactors [3–13], using intrusive and non-invasive techniques. Among these techniques, the use of optical non-invasive techniques like Particle Image Velocimetry combined with Digital Image Analysis (PIV/DIA) has been widely applied for the development, validation and verification of important correlations and their underlying assumptions reported in the literature, especially because of the relatively inexpensive experimental equipment required for the analysis [14] and the important possibility to obtain combined whole-field instantaneous information on the gas and solids phases simultaneously. On the other hand, mass transfer measurements have also been carried out using different experimental techniques, such as the use of colored gases like N_2O [15], ozone concentration measurements in a pseudo-2D bed [16,17], zirconia oxygen sensors to study nitrogen mixing in bubbles injected into incipiently fluidized beds [18] and gas exchange in 3D fluidized beds using nuclear magnetic resonance [19]. The effect of temperature on the gas exchange has also been measured experimentally by tracer gas measurements using a suction probe connected to a mass spectrometer [20]. Due to the intricate interactions between the hydrodynamics and mass exchange, it is important to obtain detailed information with high temporal and spatial resolution on the hydrodynamics and mass transfer simultaneously to understand how they affect the final performance of a fluidized bed. This is especially important for applications like drying or coating and applications with catalytic and gas-solid reactions, where the efficiency of the gas-solid contact determines the bed performance.

In general, the hydrodynamics of gas-solid fluidized beds have been studied experimentally in great detail, but an accurate numerical description of larger scale fluidized beds is still not straightforward and many underlying and simplifying assumptions (often extrapolated far from the conditions where they were validated) are still required in phenomenological models to describe the bed hydrodynamics [21–24]. Even more difficult is to accurately describe the mass exchange between the bubble and emulsion phase, which is mainly related to limitations in the techniques used until now to measure the mass exchange rates. Often the mass exchange has been measured for injected bubbles into incipiently fluidized beds using gas sampling from inside the bubbles. However, with this technique it is difficult, if not impossible, to measure gas concentration profiles inside the bubbles with high spatial resolution. Therefore, the common assumption for the numerical description of the mass transfer rate is that the gas concentration inside the bubbles is homogeneous.

For the mass transfer in gas-solid fluidized beds, the description given by Davidson and Harrison in 1963 [2] and later corrected by Rowe [15] is still accepted for single injected bubbles. Later, Sit and Grace proposed another similar description of the mass transfer phenomena for non-interacting three dimensional bubbles [16]. These correlations have been summarized in Table 1 and show that the mass exchange occurs as consequence of two different contributions, viz. gas convection through the bubble and gas diffusion from the bubble to the emulsion phase.

In addition, mass transfer in freely bubbling beds has been studied, where in general an increase in the interphase transfer as consequence of the presence of multiple bubbles is observed. Furthermore, it has also been evidenced that higher gas throughflows are expected as compared to isolated bubbles according to the observed flow distribution between the phases [28,29]. To account for this in a heuristic manner, Sit and Grace [16] used the same approach as for isolated bubbles and increased the constant in the convective term. More recently, using detailed two-fluid model simulations it has been confirmed that the gas exchange in freely bubbling beds is greatly enhanced [27].

In the last years, a novel technique based on infrared transmission has been developed and successfully applied for mass transfer measurements in fluidized bed systems [30,31], both for injected bubbles and in the freely bubbling regime. In this technique, an infrared camera is used as detector for the IR absorption by a tracer gas in pseudo 2D beds. The technique allows a much higher spatial resolution as sampling occurs in a projected area of the bed. Furthermore, it also allows a very high temporal resolution as the high-speed IR-camera is able to record images at frame rates up to 100 Hz. This technique can measure the projected instantaneous whole-field concentrations of a tracer gas inside gas voids only.

Table 1
Different correlations proposed in the literature for the mass exchange in fluidized beds.

Correlation	Conditions		References
Single bubble			
$K_{be}=\frac{4.5u_{mf}}{d_b}+\frac{5.85D_G^{0.5}g^{0.25}}{d_b^{1.25}}$	For 3D	Theoretical approach obtained using the Higbie penetration theory describing the spherical cap bubble with a 100-degree angle. The bubble has a constant size and the gas is assumed perfectly mixed	Davidson and Harrison, 1963 [2]
$K_{be}=\frac{4}{d_b}\left(\frac{2u_{mf}}{\pi}+0.6D_G^{0.5}\left(\frac{g}{d_b}\right)^{1/4}\right)$	For 2D		
$K_{be}=\frac{6.78}{1-f_w}\left(\frac{D_i\varepsilon_{mf}^2u_b}{d_b^3}\right)^{1/2}$	For 3D	Theoretical expression with uniform gas composition in the bubble and cloud using the spherical cap bubble (constant size), using the analysis from Murray to describe the flow around the bubble	Chiba and Kobayashi, 1970 [25]
$K_{be}=\frac{4.52}{1-f_w}\left(\frac{D_i\varepsilon_{mf}^2u_b}{d_b^3}\right)^{1/2}$	For 2D		
$K_{be}=\frac{1.5u_{mf}}{d_b}+12\left(\frac{D_G\varepsilon_{mf}u_b}{\pi d_b^3}\right)^{0.5}$		Expression for non-interacting three dimensional bubbles using the through flow expression from Murray (1965) and the theoretical description by Davidson and Harrison, 1963	Sit and Grace, 1981 [16]
$K_{bc}=\frac{4.5u_{mf}}{d_b}+\frac{5.85D_G^{0.5}g^{0.25}}{d_b^{1.25}}$ $K_{ce}=6.77\left(\frac{D_i\varepsilon_{mf}u_b}{d_b^3}\right)^{1/2}$ $\frac{1}{K_{be}}=\frac{1}{K_{bc}}+\frac{1}{K_{ce}}$		Use of the theoretical description by Davidson and Harrison to determine the gas exchange between the bubble phase (assumed perfectly mixed) and the cloud phase. This is a system solved in two consecutive steps: first the mass exchange between the bubble and the cloud phase and subsequently from the cloud to the emulsion phase using the Higbie penetration model	Kunii and Levenspiel, 1991 [1]
$K_{be}=0.492\varepsilon_{mf}\sqrt{u_bd_b^{1.7}}$	For 3D	Empirical correlations from injected bubbles into a bed at incipient conditions of group A and B particles	Sie and Sun, 2014 [26]
$K_{be}=0.576\varepsilon_{mf}\sqrt{u_bd_b^{1.7}}$	For 2D		
Freely bubbling beds			
$K_{be}=\frac{2u_{mf}}{d_b}+12\left(\frac{D_G\varepsilon_{mf}u_{br}}{\pi d_b^3}\right)^{0.5}$	For 3D	Expression for interacting 3D bubbles using the through-flow expression from Murray (1965) and the theoretical description by Davidson and Harrison, 1963, and corrected by the increase in the through-flow gas	Sit and Grace, 1981 [16]
$K_{be}=\frac{9u_0}{4d_b}$	For 2D	For Geldart B particles using potential flow theory for gas through-flow, ranging up to u/u_{mf} of 3. Note that superficial gas velocity (u_0) is used in the correlation instead of u_{mf}	Hernandez et al, 2013 [27]

The present work aims at extending the application of the technique for mass transfer measurements for first injected bubbles into an incipient fluidized bed, which is subsequently extended to freely bubbling beds. The measurements have been carried out under different experimental conditions to better understand the mass transfer phenomena, in particular different particle sizes, particle densities and bubble injection velocities. First, the experimental setup and the fundamentals of the applied IR-technique are described. Then, a new method to accurately determine the amount of particles inside the bubbles and subsequent bubble reconstruction is proposed. After the description of the main improvements to the analysis of the IR images, the results of the mass transfer measurements are presented and discussed, and the experimental findings are compared in detail with available correlations from the literature. Finally, a general summary with the main conclusions obtained in this work is presented.

2. Experimental

2.1. Description of the technique and the experimental setup

Any material with a temperature above 0 K emits infrared radiation and this can be measured with an IR-camera equipped with specific detectors. The vibrational frequencies of many molecular bonds like C═O or C—H lay in the IR wavelengths. When a gas with these bonds is exposed to IR radiation, the molecules absorb part of the IR implying a transition of the molecular vibration to an excited vibrational state with a corresponding change in the dipole moment. An IR camera is able to measure the decrease in the IR radiant flux associated with the absorption by the gas molecules and this property is used in this study for the measurement of mass transfer in fluidized beds.

The IR absorption at low concentrations can be described by Lambert Beer's law (Eq. (1)), where the absorbance (A) is proportional to the gas concentration (C), the target length (ℓ) and the molecular absorbance (ε). The absorbance can be also determined through the decrease in intensity caused by the exposure of a gas to IR radiation. The absorbance (as defined by Eq. (2)) and transmittance (defined in Eq. (3)) are used for the measurement of gas concentrations.

$$A=-\varepsilon\ell C=aC \tag{1}$$

$$A=-\ln\frac{I}{I_0} \tag{2}$$

$$T=\frac{I}{I_0} \tag{3}$$

In these equations I_0 refers to the IR intensity measured by the detector in absence of any gas absorbing IR radiation (it is here referred to as the background image), while I is the intensity measured by the detector when an absorbing gas is exposed to the IR source. At higher concentrations, deviations from Lambert Beer's law can be expected, but the decrease in intensity can be calibrated to the gas concentration and subsequently used for the study of mass transfer rates in fluidized beds.

The experimental setup used in this study (depicted in Fig. 1) consists of three elements perpendicularly positioned to enhance the resolution of the technique. These elements refer to the IR source, the detector (IR camera), and the fluidized bed column. A detailed discussion on the selected system can be found in a previous work [31]. The IR source is an anodized aluminum plate kept at 430 °C with 300 × 150 × 20 mm in height, width and depth respectively. The IR camera is aligned perpendicularly to the IR source. The camera (SC7650 FLIR Systems) has an Indium Antimonide (InSb) detector for IR emission and is able to measure in a spectral range from 1.5 to 5.1 μm wavelengths with a maximum resolution of 640 × 512 pixels and 100 Hz frame rate. The window

size of the IR images presented in this paper is always between 8×12 and 12×18 cm^2 (width $\times$ height). An IR filter made of sapphire (supplied by Edmund Optics) has been mounted inside the IR camera in order to cut off and restrict the target wavelength. This filter has a central wavelength at 3.46 μm and provides 80% transmittance. The main purpose of the filter is to increase the resolution in the detection of the tracer gas used in this work, propane (C_3H_8), which shows a strong absorption peak at this wavelength associated to the C—H bonds.

The column is made of quartz, which has a high transmittance (>80%) at the targeted wavelengths, and has a total height of 500 mm, 200 mm in width and 4 mm in depth. The quartz column is coupled to a stainless steel chamber, where the porous plate distributor (40 μm pore size) and the points for bubble injection are located.

Tracer gas bubbles are injected into the column through a solenoid valve (ASCO 262) connected to a control system for the opening time and frequency of injection. The solenoid valve is connected in turn to a pressurized vessel to assure a constant injection pressure. Gas coming from the solenoid valve is injected into the reactor through a close-end tube with an orifice pointing upwards. Injectors with orifices of 1 and 2 mm have been built to modify the velocity of the injected gas. N_2 is used as background gas and is fed via the porous plate distributor to keep the bed at incipient (or freely bubbling) conditions.

The procedure for the measurements has been summarized and optimized in a previous work [31], where the reproducibility and reliability of the measurements were assessed in detail. First, the absorbance is calibrated for different gas compositions in single gas phase (no particles). Subsequently, the two phase (fluidized bed) calibration procedure method is used, where a background image (I_0) is obtained by composing an image from the bubbles in a fluidized bed fed with pure N_2. Finally bubbles are injected into the bed and the absorbance (thus concentration) is determined through the intensities (I) measured inside the bubbles and the former calibration. However, when a known concentration is fed to the two-phase reactor, a small discrepancy in the measured concentration is still observed, which can be attributed to two different effects. The first cause is related to the method used to detect particles inside the bubbles and how these particles were removed from the analysis. In the work by Dang et al. [30] the particles inside the bubbles have been removed by determining the center of the particle and the subsequent removal of pixels in the neighborhood. The second cause is associated with the bubble diameter used for the determination of the background image and the comparison to the diameter of the injected bubble. The bubble diameter is related to the opening of the bubble and thus to the intensity measured by the detector, i.e. intensities measured inside two bubbles with two different diameters are slightly different as they behave like a diaphragm of optical cameras. Both effects have been corrected for and the accuracy of the measurements has been improved in this work. The post processing of the data is done in Matlab using an in-house code developed for the measurement of gas concentration profiles from IR images. A more detailed description on the new methodology developed in this work is given in the next sections (Sections 2.2 and 2.3).

Mass transfer measurements have been carried out for injected bubbles into a bed at minimum fluidization conditions and into a freely bubbling bed and a summary of the main conditions studied in this work are shown in Table 2. The analysis methods used to determine the bubble-to-emulsion phase mass transfer coefficient is described subsequently in Sections 2.4 and 2.5.

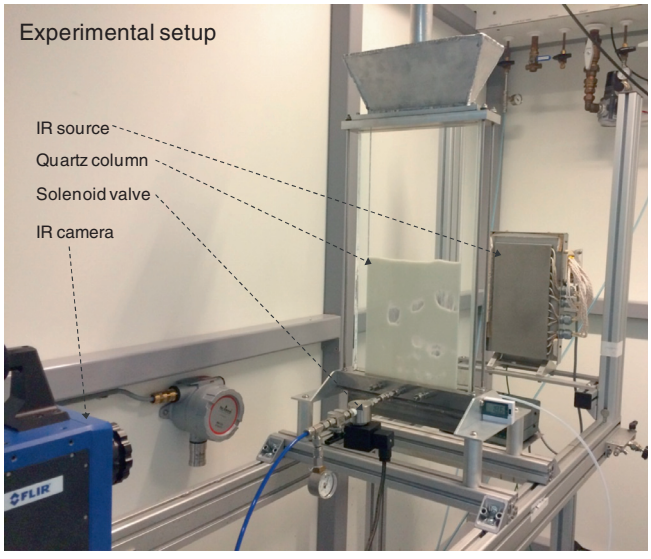

Fig. 1. Picture of the experimental facility used in this study for the measurement of mass transfer in fluidized beds through injected bubbles into a bed at incipient conditions or freely bubbling beds.

2.2. Description of a new method for particle detection inside the bubbles

Dang et al. [30] developed a method where particles inside bubbles are detected and removed based on the much higher IR absorption of the particles compared to the tracer gas. However, the edges of the particles produce scattering of the IR emission with absorbance in the range of the gas phase. Dang et al. [30] removed the particle scattering by filtering a relatively large area of 7px by 7px from the center of the particles. With this method a relatively large part of the concentration measurement in the gas bubbles is lost due to the high coverage of this filter. On the other hand, if smaller filtering areas were used, not all the scattering would have been removed affecting the accuracy of the concentration measurement.

In the new method, also first the center of mass of the particles is determined (Fig. 2a). At the detected particle centers, the particle absorbance is artificially increased to a very high value and the gradients between the center of mass and the particle surroundings are determined (Fig. 2b). The thus determined gradients are much higher than the gradients associated with the tracer concentration profiles in the gas phase, so that the isocontours (defined at a relative intensity of one/two order(s) of magnitude higher than gradients of tracer gas concentration profiles) correspond to the edges of the particles including their scattering. With this method the radiation from the particles and the scattering caused by the particles can be selectively removed from the IR-image, as depicted in Fig. 2c, while the information on the concentration profiles in the gas phase is not modified. By combining the information from the center of the particles and their scattering, it is possible to subtract the particles from the measurements more accurately and with a much smaller filter than before (Fig. 2d).

2.3. Improvement of the background correction method

The bubble diameter, namely aperture of the bubbles, modifies the IR intensity measured in the detector as they behave as lenses for the detector. When a background image is being composed, it obviously consists of big and small bubbles that give slightly different intensities at similar positions in the bed. This effect would result in a systematic error when measuring the concentration inside the injected bubble. In order to correct/decrease this error, a new method is developed that classifies every bubble according to its diameter in bins and uses a calibration curve for that diame-

Table 2
List of experimental conditions selected in this work for the study of mass transfer rates for injected bubbles into a bed at incipient conditions and into the freely bubbling regime.

Particle type	Mean particle diameter (μm)	Injection time (ms)	Injection pressure (bar)	u_{mf} experimental (m/s)	Superficial gas velocity u_0/u_{mf}
Glass beads	650	20–45	2–4	0.30	1–2
Glass beads	500	20–35	2–4	0.21	1–2
Glass beads	400	18–32	2–4	0.15	1–2
Glass beads	250	18–30	2–4	0.09	1–2

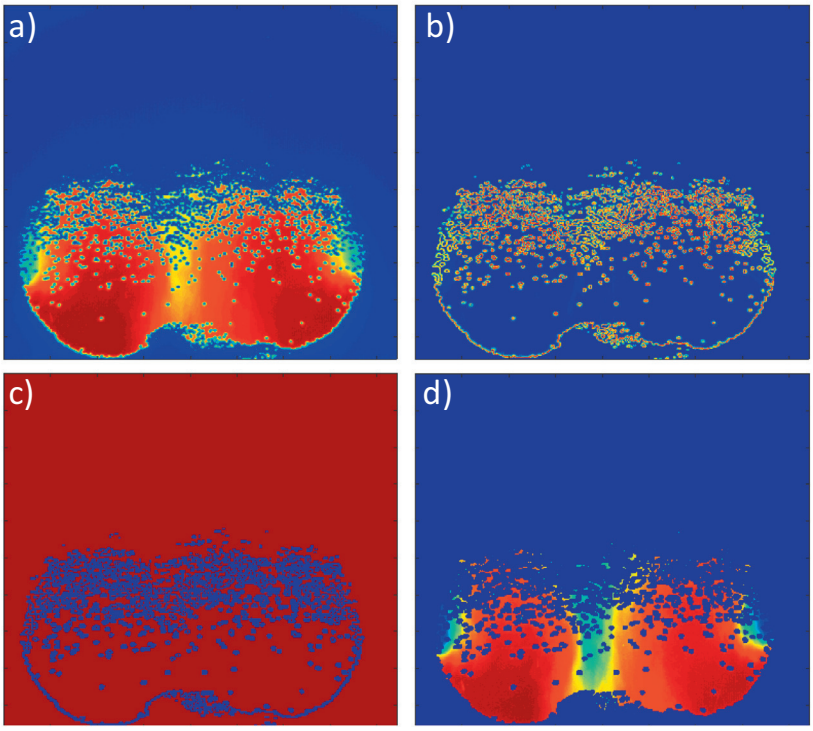

Fig. 2. Procedure for accurate particle detection and removal from the IR image; a) original image; b) gradients due to scattering; c) binary image generated based on the gradients; d) resulting image after particle filtering.

ter bin. By composing a background image using bubbles with similar sizes, a more homogeneous distribution of intensities is obtained. In total three different background images are acquired, namely small bubbles (1–3 cm), intermediate bubbles (3–5 cm) and big bubbles (>5 cm). When a bubble is injected into the incipiently fluidized bed, first its diameter is determined and the absorbance is calculated by subtracting its corresponding background image. The validation of the method has been carried out by feeding known concentrations of the tracer gas C_3H_8 and subsequent comparison of the concentration measured according to the new and old method (that used only a single background image). Results of this validation are given in Table 3, clearly showing that the results are much improved when using three background images.

2.4. Reconstruction of the whole field concentration profiles in bubbles

When giving a closer look at the IR images, it is observed that bubbles are much bigger than the visible projected area covered by the gas phase inside the bubbles. This is a consequence of (some time severe) particle raining inside the bubble and, especially important, at the edges of the bubbles, and in particular at the roof of the bubbles. Mass exchange measurements trace the volume-averaged tracer gas concentration inside a bubble as a function of time. However, since an important part of the bubble is blocked from sight by the raining particles, the measured averaged tracer gas concentration would deviated from the actual averaged concentration. Therefore, in this work a concentration profile reconstruction algorithm has been developed in order to interpolate the gas phase concentrations in the areas covered by the particles inside the bubbles.

At first, the algorithm determines the center of mass of the bubble (Fig. 3a). Bubbles are distinguished from the emulsion phase by normalizing the image based on the IR emission intensity detected by the IR camera and converting it into a binary image using a threshold value to distinguish the emulsion and bubble phases (relative gradient pixel intensity above 0.2 is defined as bubble phase), similar as used in other image-based techniques like digital image analysis (DIA). The resulting image after particle removal is

Table 3
Comparison of the accuracy when using the previous background correction method and the new method using three background images related to different bubble diameters.

Propane concentration fed in the column (mol/L)	Relative deviation (%)	
	Old method	New method
0.0025	64.0	27.3
0.0045	38.3	8.99
0.0065	9.59	5.58
0.0085	5.02	4.98
0.0115	9.78	2.47

then overlapped with the detected bubble (Fig. 3b), thus defining the area missing for the whole-field bubble concentration reconstruction. The algorithm to reconstruct the gas concentration profiles inside the bubbles starts at the determined center of mass of the bubble. The algorithm carries out a pixel-per-pixel screening inside the bubble following a trajectory from the center of the bubble towards the bubble edges. If during the screening a pixel defined as bubble phase with certain concentration is encountered, the algorithm jumps to the next pixel until it finds a pixel not defined as bubble phase. This pixels is surrounded by eight adjacent pixels, and it takes the average value of all these adjacent pixels excluding the adjacent pixels that are not defined as bubble phase, if any, that will subsequently be interpolated during the screening process (and eventually using the previously interpolated pixel position). If the center of mass corresponds to a position detected as particle and is surrounded by pixels defined as particles, the method is repeated as many times as needed in order to substitute all not bubble phase pixels inside the bubble. When this reconstruction algorithm is applied to the image, the resulting image (shown in Fig. 3c) can describe the concentration profiles inside the bubbles fairly accurately. This reconstruction results in a more accurate average tracer gas concentration inside the bubbles and reduces the deviation in the measurements since particles inside the bubbles caused by particle raining are located at somewhat arbitrary places, which for non-reconstructed images leads to noisier average tracer gas concentrations in time. Only for those cases where the particle raining is too excessive the method cannot reconstruct the gas concentration profiles inside bubbles accurately and these cases were not considered for further data analysis.

2.5. Analysis method for mass exchange coefficient determination in fluidized beds

The bubble-to-emulsion phase mass transfer rates include contributions from two terms, namely gas convection and gas diffusion. The convective term refers to the gas that enters the bubbles from the bottom and leaves at the top of the bubble and is more important for larger particles. The diffusive term is dominated by molecular diffusion of the gas from the bubbles to the emulsion phase and is more dominant for smaller particles. Mass transfer rates have been measured in the literature by solving the mass balance of the tracer gas inside the bubbles. In general, three main approaches have been used when determining mass transfer rates for stable bubbles. The first one proposed by several authors [2,32] neglects the presence of the cloud in the bubbles. In this case the gas exchange occurs directly between the bubble and the emulsion phases. The second method assumes that the cloud and the bubble phases behave like a single well mixed phase and gas exchange occurs between this phase and the emulsion phase, mainly through molecular diffusion [33,34]. The third method, and most used in the literature, is the approach suggested by Kunii and Levenspiel. This method also includes a resistance to mass transfer from the bubble to the cloud phase [1].

For the different approaches, the data generated from the measurements is used similarly to solve general mass balances for the different included phases. Following the first approach, the integral unsteady mass balance for the tracer gas inside the bubbles is given in Eq. (4).

$$\frac{d(C_{t,b}V_b)}{dt} = -K_{be}(C_{t,b} - C_{t,e})V_b \tag{4}$$

In order to determine the volumetric bubble-to-emulsion phase mass transfer coefficient K_{be}, the averaged tracer gas concentration inside the bubbles and the bubble volume is measured as a function of time. The IR method only allows for the measurement of the gas concentrations inside the bubbles and cannot determine the concentrations in the emulsion phase. Therefore, the following initial conditions and assumptions are used in the analysis of the experiments in this work:

$$C_{t,b} = C_{t,0} \ at \ t = 0$$
$$V_b = V_{b,0} \ at \ t = 0$$
$$C_{t,e} \approx 0$$

For the analysis it is assumed that the tracer gas concentration in the emulsion phase can be neglected. Since the dense phase absorbs all the IR radiation emitted by the IR source, it is not possible to measure gas concentrations in the emulsion phase, and therefore, we need an assumption for the emulsion phase concentration. The assumption that the emulsion phase concentration is negligibly small, is supported by the fact that the experiments do not show any reentrance of tracer gas at the bottom of the bubble by convection. This would indeed be expected according to potential flow theory and the limit of penetration for the gas streamlines in the bubbles as represented in the work of Davidson and Harrison [2]. In this case the gas leaving the bubble from the top would be dragged downwards by the particles in the cloud region towards the wake of the bubble. Afterward, this gas would enter again inside the bubble by gas convection. Since this behavior is not observed experimentally, the given assumption can be considered for the analysis.

Integrating Eq. (4) leads to Eq. (5)

$$\frac{C_{t,b}(t)V_b(t)}{C_{t,b,0}V_{b,0}} = \exp(-K_{be}t) \tag{5}$$

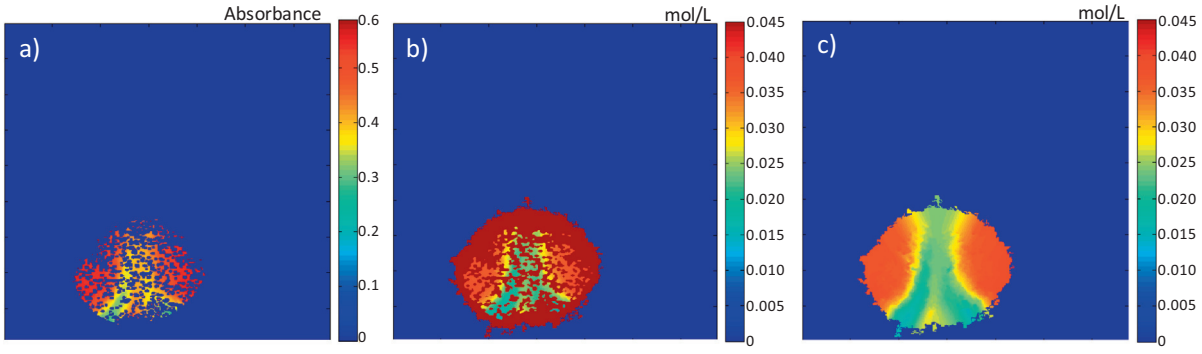

Fig. 3. Bubble reconstruction by substitution of the particle phase inside the bubbles by tracer gas phase concentration; a) image after particle removal; b) tracer gas concentration profiles inside the bubble; c) reconstructed concentration profile inside the bubble.

And since the results are obtained in a pseudo 2D reactor, Eq. (5) can be written as Eq. (6):

$$\frac{C_{t,b}(t)}{C_{t,b,0}}\left(\frac{D_b(t)}{D_{b,0}}\right)^2 = \exp(-K_{be}t) \quad (6)$$

The overall mass transfer coefficient can be determined by the negative of the slope when plotting the logarithm of the term on the left hand side in Eq. (6) as a function of time.

3. Results

3.1. Bubble injection into a bed at minimum fluidization conditions

As an example of typical results obtained with the IR-transmission technique, Fig. 4 presents the evolution of an injected bubble with a tracer gas concentration of 0.045 mol/L into a bed consisting of 400 μm glass beads at incipient conditions at different moments in time after bubble injection. At first, during the period of bubble formation, the bubble is full of tracer gas. Once the injection is finished and the bubble becomes stable in the bed, mass exchange between the tracer gas in the bubble phase and the N_2 flowing through the emulsion phase at minimum fluidization conditions occurs. From the figure a first period of gas exchange corresponding to N_2 convection through the middle of the bubble is observed. Afterwards, diffusion through the perimeter of the bubble to the emulsion phase takes place.

The mass exchange rates can be subsequently calculated from the unsteady bubble phase mass balance for the injected bubbles. A common representation of the data analysis in terms of change in bubble concentration as function of time (Eq. (6)) is presented in Fig. 5. From this figure, the slope of the linear trend represents gives the mass exchange coefficient (K_{be}). In this work, it was possible to adjust the size of the injected bubble by tuning the injection pressure and the opening time of the valve, creating thus a wide range of operating conditions. For all the experimental conditions several bubbles of the same size (at least eight) were injected to verify reproducibility of the results, where the measured standard deviation of the determined K_{be} values for each set of experimental conditions was found to be around 10%. The mass transfer coefficients measured for the different selected experimental conditions listed in Table 2 as a function of the bubble size is given in Fig. 6. In addition, the mass transfer rates have been compared with the theoretical correlation given by Davidson and Harrison and a good agreement is observed in general, with a somewhat larger difference for the bigger particles. A more detailed explanation of the occurring phenomena and the observed deviations will be given in the discussion section.

3.2. Bubble injection into a freely bubbling bed

Mass transfer rates in freely bubbling beds have also been measured experimentally with the IR technique. In this case, bubbles are injected into a bed operated above the minimum fluidization conditions, thus in the presence of other bubbles with which the injected bubble interacts. For all cases the maximum superficial gas velocity used corresponds to two times u_{mf} to avoid the formation of very big bubbles approaching the width of the column, which strongly hampers the interpretation of the results due to wall effects. The procedure followed to determine the volumetric mass exchange coefficients is the same as presented and used in the previous sections.

For the bubbles injected into a freely bubbling bed, it is observed that tracer gas from the injected bubble rapidly moves to an adjacent upstream bubble due to the increased through-flow. This mechanism was expected according to potential flow theory, but is now actually visualized. Fig. 7 shows the evolution of the concentration field inside an injected bubble at different moments in time and shows how the tracer gas enters a second bubble situated above it. The increase in the gas through-flow increases the mass exchange rates. Many experiments have been carried out with different injected bubble volumes and for beds consisting of particles of different diameter. In many of these experiments the injected bubble coalesced with another bubble present in the bed, and these cases were excluded from the analysis, so that only stable bubbles without break-up or coalescence during the recording time have been considered (see Fig. 7 as an example). The exchange rates measured experimentally have first been compared with the theoretical description for isolated bubbles since this is still very often used in phenomenological models of fluidized beds reported in the literature [35–37]. However, as shown in Fig. 8, a mismatch is observed corresponding to the clear enhancement of the mass transfer rates in freely bubbling bed conditions (even up to a factor of 2). This is further discussed in the next section.

4. Discussion

4.1. Mass transfer in a bed at incipient conditions

The volumetric bubble-to-emulsion phase mass exchange coefficients determined from the experiments are in good agreement with the theoretical predictions by Davidson and Harrison [2] for 2D beds. For the case of 650 μm particles the variation in the experimentally determined exchange coefficients was relatively large, which may be attributed to instabilities in the bubble shape or to the limited number of particles in the depth of the column (i.e. wall effects). For all other particles the measured mass exchange coefficients tends to be slightly lower than the theoretical predictions. Two different causes may be responsible for this discrepancy: 1) the injected bubbles of propane are heavier than the N_2 in the emulsion phase and are also travelling at velocities higher than those in the emulsion phase, which could cause an increased resistance to gas diffusion, and 2) the theoretical values are computed based on the underlying assumption that the velocity profiles are the same as those obtained from potential flow theory for an isolated bubble rising through an unconfined emulsion phase at incipient fluidization conditions. This assumption is clearly not fully valid for the here considered cases, since the velocity distribution is somewhat distorted due to the bubble injection in the bed.

To verify the first hypothesis, experiments have been carried out using a different background gas. Experiments with 400 μm glass beads have been repeated using He (with a much lower density than C_3H_8) and CO_2 (similar density) instead of N_2, and also these results have been compared to the predictions from the theoretical correlation (see Fig. 9). The results clearly indicate that the density difference between the tracer gas and the background fluidization gas does not affect the determined mass exchange coefficients. All the experimentally determined exchange coefficients are similar and indeed slightly lower than the theoretical values, which indicates that the observed discrepancies are most likely related to the assumptions on the velocity distribution around the bubbles.

The second hypothesis suggests that a different bubble rise velocity is used in the derivation compared to the bubble rise velocity in the corresponding experiments. This has been verified experimentally by analyzing the bubble velocity through the displacement of the center of mass of the injected bubbles and comparing the obtained rise velocities with the bubble rise velocity used in the correlation proposed by Davies and Taylor [38] and

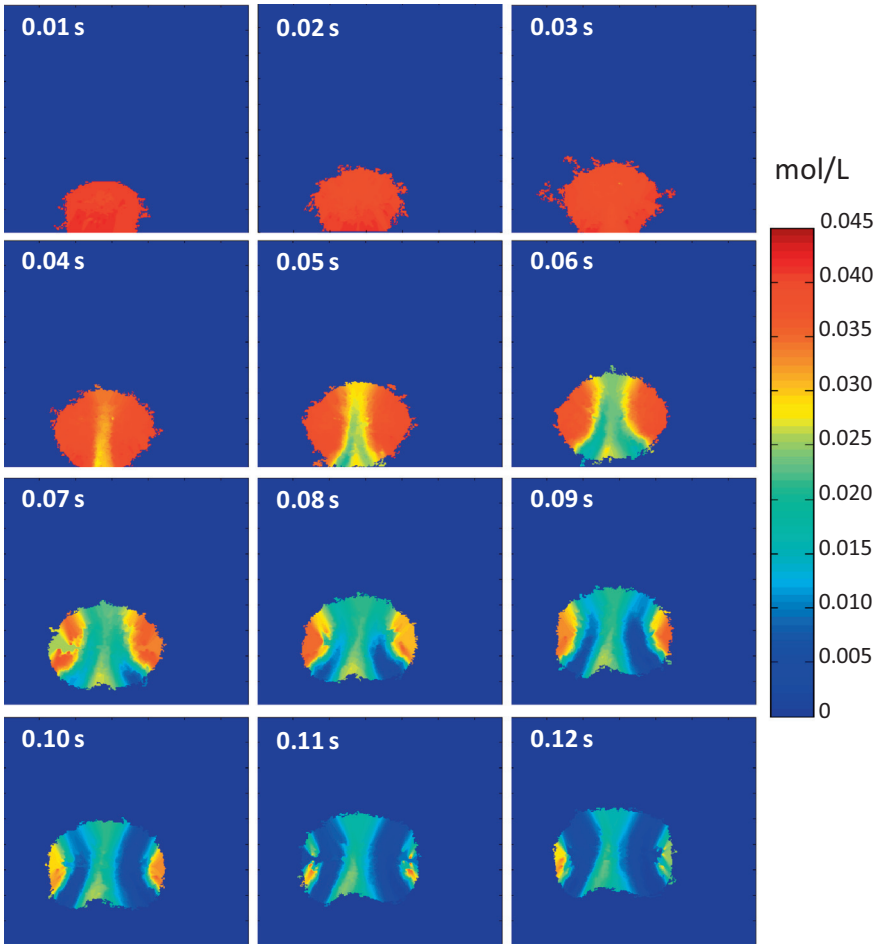

Fig. 4. Tracer gas concentration profiles (in mol/L) inside bubbles as a function of time for an injected bubble in an incipient bed filled with 400 μm glass beads.

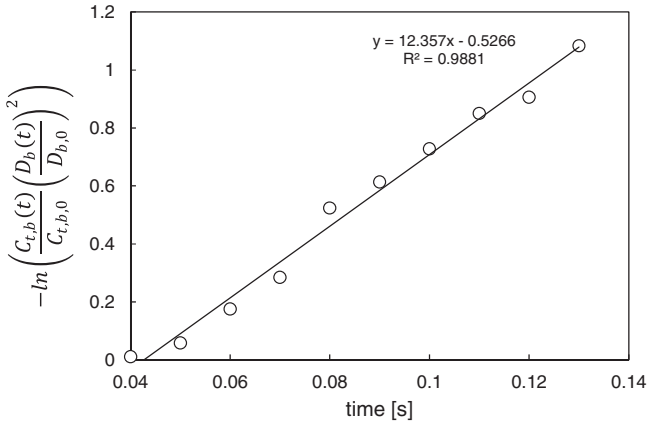

Fig. 5. Change in average tracer gas concentration inside the bubble as function of time (Eq. (6)) for a bubble of 4.4 cm injected into an incipient bed of particles with a mean diameter of 500 μ.

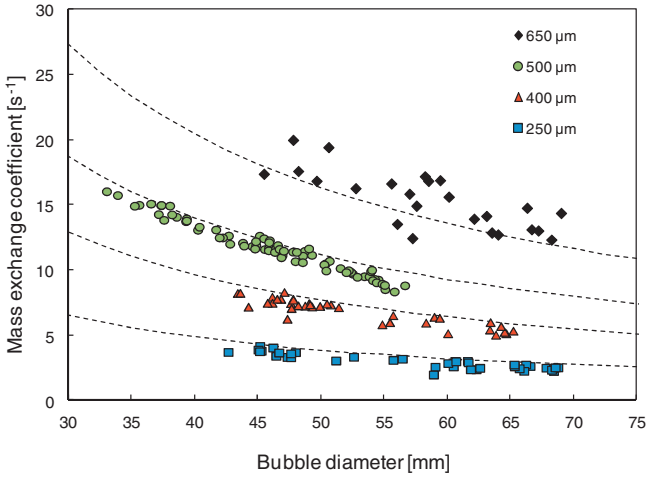

Fig. 6. Experimentally determined bubble-to-emulsion phase mass exchange coefficients for different particle sizes and bubble diameters using the IR technique. The dashed lines represent theoretical predictions from the correlation by Davidson and Harrison for 2D beds [2].

summarized by Kunii and Levenspiel [1]. The results of this analysis are depicted in Fig. 10.

The results show that for all the particle sizes the measured bubble rise velocity is always significantly lower than the computed value from the correlation assumed in the theoretical derivation of K_{be}, and the discrepancy increases in time. This can be attributed to bubble deformation which was clearly visible in the experiments (see also Fig. 4). The bubbles become less spherical/spherical cap and adopt an ellipsoid form, which leads to shorter displacements of the centers of mass measured at each moment in time. Giving a closer look at the derivation of the diffusion term in the correlation by Davidson and Harrison [2], one can note that the Davies and Taylor [38] expression is used

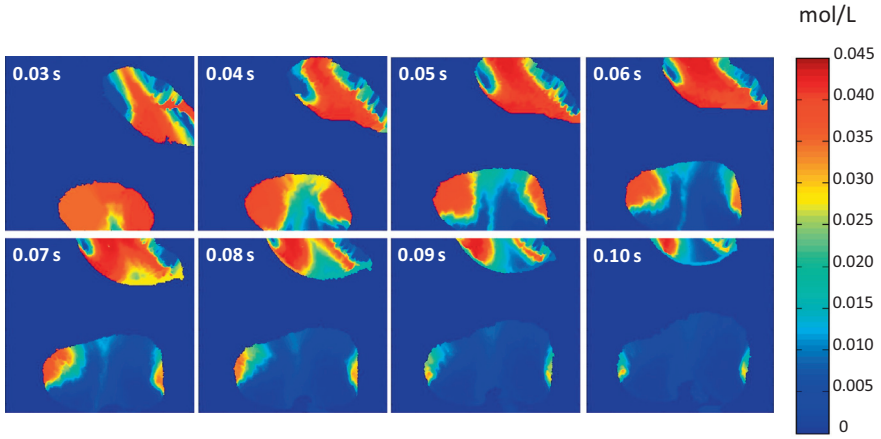

Fig. 7. Tracer gas concentration profiles (in mol/L) inside bubbles at different moments in time for a bubble injected into a freely bubbling bed consisting of 400 μm glass beads operated at 1.5 u_{mf}.

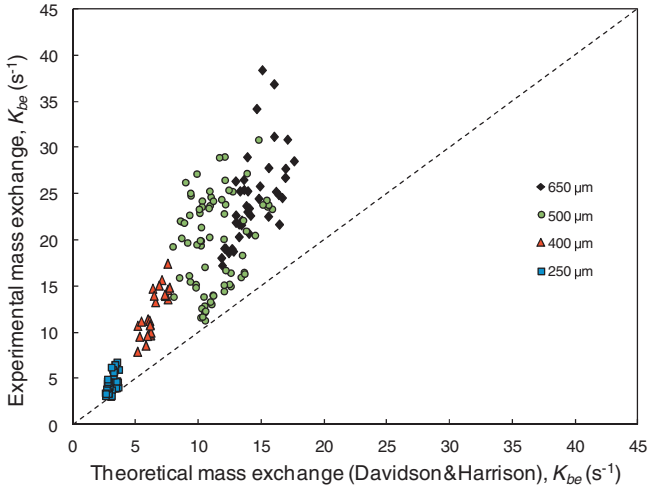

Fig. 8. Parity plot of experimentally determined mass exchange coefficients (K_{be}) using the IR technique and theoretically estimated values for 2D beds [2] for different particle sizes (indicated with different markers) and bubble diameters in a freely bubbling bed.

for the bubble rise velocity. Since in the work presented in this study the measured bubble rise velocity is much lower, it implies that the diffusion contribution is smaller than theoretically predicted. Therefore, the mass transfer rates observed are always lower than the theoretical mass transfer rates. However, since the experiments are carried out at room temperature and the minimum fluidization velocity for all the particles is rather high, the diffusion contribution is much lower in comparison to the convective contribution. Therefore, the discrepancies observed in K_{be} are rather small for all the particle sizes considered. Furthermore, the smaller the u_{mf}, the smaller the contribution of the convective term compared to the diffusion term. This is also observed experimentally for the results for the 250 μm particles, where the deviation is somewhat larger than for the other particles since the diffusion term has more weight in the overall mass exchange rate compared with the other particles, where the deviation becomes smaller. Thus, the small deviations can most likely be attributed to discrepancies in the bubble rise velocity, whereas it can be confirmed that the technique gives representative results of the mass transfer rates in fluidized beds.

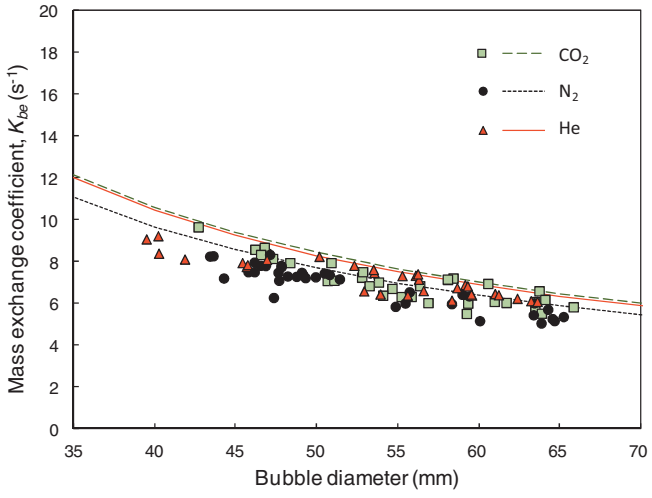

Fig. 9. Experimental mass transfer rate coefficients for different background gases using the IR technique. The dashed lines represent the theoretical K_{be} as calculated using the correlation by Davidson and Harrison in 2D beds [2].

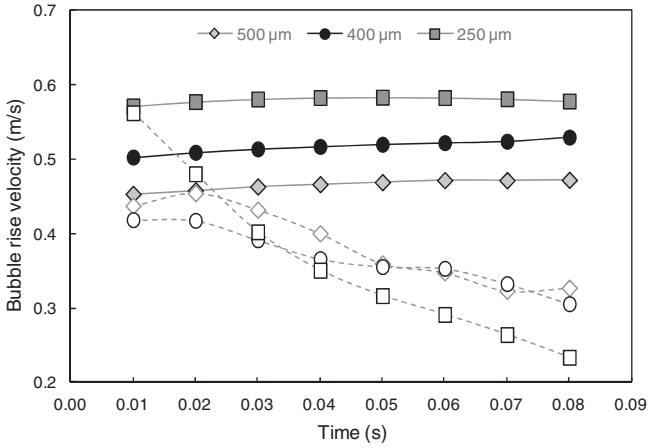

Fig. 10. Comparison of the bubble rise velocity as a function of time measured for the injected bubbles using the IR-technique (empty markers) with the theoretical predictions [1] for the experiments with different particle sizes (filled markers).

4.2. Mass transfer in a bed in the freely-bubbling regime

A remarkable difference between the experimentally measured mass exchange coefficients with the theoretically predicted mass exchange coefficients for isolated bubbles has been observed for the case of injected bubbles into a freely bubbling bed, as reported in Fig. 8. This confirms experimentally the theoretical approach described by Sit and Grace [16], who increased the convective contribution to account for the increased through-flow. In this study, it is now possible to fit the experimental data to a correlation that can describe the mass transfer rate between the bubble and emulsion phase in freely bubbling fluidized beds more accurately. To this end, the equation proposed by Davidson and Harrison is used as reference, where the constant terms for the convective and diffusive terms have been adjusted. In this fitting it is observed that the diffusive part can indeed be neglected and that the gas exchange has only a convective contribution. This fact has also been noted by Hernandez et al. [27], who observed from CFD simulations that the mass exchange in bubbling beds is only related to gas convection and that it depends on the superficial gas velocity (instead of the minimum fluidization velocity).

Following the same approach as proposed by Hernandez et al. [27], the data has been fitted to an equation of the same type. The resulting equation to describe the bubble-to-emulsion phase mass transfer rate in bubbling regime is presented in Eq. (7). This equation minimizes the total error for all the experiments carried out with different particle sizes, bubble diameters and superficial gas velocities. A parity plot with the experimental mass exchange coefficients and the calculated values according to Eq. (7) is reported in Fig. 11. In this figure it is observed that the maximum deviation for the measurements is around 20%, whereas for most of the experimental conditions the error is even within 10%.

$$K_{be} = \frac{4}{d_b}\left(\frac{2.6u_0}{\pi}\right) \quad \textit{Fitted data} \tag{7}$$

It is worth remarking that the fact that the mass transfer rate in freely bubbling beds is much higher than for isolated bubbles and that it depends on the superficial gas velocity, has an important implication for systems with heterogeneously catalyzed reactions with molar gas expansion, like in fuel reforming reactions. These systems are often limited by bubble-to-emulsion phase mass transfer, since the reaction kinetics are relatively fast [39]. In studies that use the Kunii and Levenspiel correlations based on correlations for single bubbles to describe the bubble-to-emulsion phase mass transfer rate, the mass exchange is likely to be significantly underestimated. This clearly indicates the need to further enhance the phenomenological models with improved correlations with extended validity ranges, which can now be developed making use of novel experimental techniques.

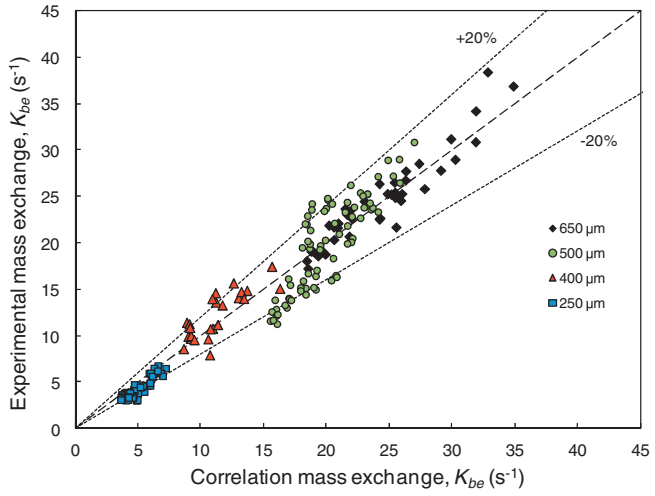

Fig. 11. Comparison of the mass exchange coefficient measured experimentally with the IR technique in a freely-bubbling bed and the correlation developed in this work (Eq. (7)).

5. Conclusions

Gas exchange coefficients have been experimentally determined using the recently developed IR transmission technique for single bubbles injected into a bed at incipient and freely-bubbling fluidization conditions, using propane as tracer gas and N_2 as background fluidization agent. In this work, the gas concentration profiles inside the bubbles have been reconstructed from the original images improving the determination of the volume-averaged bubble concentration and thus also the bubble-to-emulsion phase mass transfer coefficients. In addition, the technique allows a visualization of the mass transfer processes, which helps to analyze and improve the underlying assumptions in the derivation of mass transfer correlations for phenomenological models.

The experimental results have shown that the theoretical description given in the early 60's by Davidson and Harrison apply well for mass exchange from isolated bubbles at room temperature conditions. For bigger particles a somewhat larger variation in the data was observed, probably related to shape deformation or wall effects. The experimentally determined bubble-to-emulsion phase mass transfer coefficients are somewhat lower than the theoretical predictions, and it was shown that this is not caused by density differences between the tracer gas and the background fluidization gas, but rather to differences in the bubble rise velocity that was experimentally measured vs. the correlation assumed in the correlation.

For injected bubbles into freely bubbling beds the experiments have shown a considerable increase in the bubble-to-emulsion phase mass transfer coefficients in comparison to isolated bubbles injected into fluidized beds at incipient conditions, which could be clearly attributed to the increased through-flow of gas passing through the bubble. The experimentally generated data have been used to develop an empirical correlation able to predict accurately (with deviations within 20%) the gas exchange based on the bubble size and superficial gas velocity, where it should be noted that the convection term was dominant for the cases considered in this work. Finally, it is stressed here that many gas-solid fluidized beds are operated at elevated temperatures and that the study on mass transfer therefore also needs to be extended to fluidization at high temperatures.

Acknowledgments

NWO/STW is acknowledged for the financial support through the VIDI project number 12365.

References

[1] D. Kunii, O. Levenspiel, Fluidization Engineering, second ed., 1991.
[2] J.F. Davidson, D. Harrison, Fluidised Particles, Cambridge University Press, New York, 1963.
[3] S. Maurer, E.C. Wagner, T.J. Schildhauer, J.R. van Ommen, S.M.A. Biollaz, R.F. Mudde, X-ray measurements of bubble hold-up in fluidized beds with and without vertical internals, Int. J. Multiph. Flow 74 (2015) 118–124.
[4] M. Kashyap, B. Chalermsinsuwan, D. Gidaspow, Measuring turbulence in a circulating fluidized bed using PIV techniques, Particuology 9 (2011) 572–588.
[5] C.R. Müller, J.F. Davidson, J.S. Dennis, P.S. Fennell, L.F. Gladden, A.N. Hayhurst, M.D. Mantle, A.C. Rees, A.J. Sederman, Oscillations in gas-fluidized beds: ultra-fast magnetic resonance imaging and pressure sensor measurements, Powder Technol. 177 (2007) 87–98.

[6] M. Stein, T.W. Martin, J.P.K. Seville, P.A. McNeil, D.J. Parker, Chapter 10 – positron emission particle tracking: particle velocities in gas fluidised beds, mixers and other applications, in: J.C.L.P. Duduković (Ed.), Non-Invasive Monit. Multiph. Flows, Elsevier Science B.V, Amsterdam, 1997, pp. 309–333.
[7] M.S. Fraguío, M.C. Cassanello, F. Larachi, S. Limtrakul, M. Dudukovic, Classifying flow regimes in three-phase fluidized beds from CARPT experiments, Chem. Eng. Sci. 62 (2007) 7523–7529.
[8] S. Liu, Q. Chen, H.G. Wang, F. Jiang, I. Ismail, W.Q. Yang, Electrical capacitance tomography for gas–solids flow measurement for circulating fluidized beds, Flow Meas. Instrum. 16 (2005) 135–144.
[9] K.A. Buist, A.C. van der Gaag, N.G. Deen, J.A.M. Kuipers, Improved magnetic particle tracking technique in dense gas fluidized beds, AIChE J. 60 (2014) 3133–3142.
[10] C. He, X.T. Bi, J.R. Grace, Monitoring electrostatics and hydrodynamics in gas-solid bubbling fluidized beds using novel electrostatic probes, Ind. Eng. Chem. Res. 54 (2015) 8333–8343.
[11] J.R. van Ommen, S. Sasic, J. van der Schaaf, S. Gheorghiu, F. Johnsson, M.-O. Coppens, Time-series analysis of pressure fluctuations in gas–solid fluidized beds – a review, Int. J. Multiph. Flow 37 (2011) 403–428.
[12] J.F. de Jong, M. van Sint Annaland, J.A.M. Kuipers, Experimental study on the hydrodynamic effects of gas permeation through horizontal membrane tubes in fluidized beds, Powder Technol. 241 (2013) 74–84.
[13] J.A. Medrano, R.J.W. Voncken, I. Roghair, F. Gallucci, M. van Sint Annaland, On the effect of gas pockets surrounding membranes in fluidized bed membrane reactors: an experimental and numerical study, Chem. Eng. J. (2015).
[14] J. Laverman, I. Roghair, M. van Sint Annaland, J.A.M. Kuipers, Investigation into the hydrodynamics of gas–solid fluidized beds using particle image velocimetry coupled with digital image analysis, Can. J. Chem. Eng. 86 (2008) 523–535.
[15] P.N. Rowe, B.a. Partridge, Cloud formation around bubbles in gas fluidized beds, Chem. Eng. 19 (1964) 973–985.
[16] S.P. Sit, J.R. Grace, Effect of bubble interaction on interphase mass transfer in gas fluidized beds, Chem. Eng. Sci. 36 (1981) 327–335.
[17] S.P. Sit, J.R. Grace, Interphase mass transfer in an aggregative fluidized bed, Chem. Eng. Sci. 33 (1978) 1115–1122.
[18] R. Solimene, A. Marzocchella, G. Passarelli, P. Salatino, Assessment of gas-fluidized beds mixing and hydrodynamics by zirconia sensors, AIChE J. 52 (2006) 185–198.
[19] T. Pavlin, R. Wang, R. McGorty, M.S. Rosen, D.G. Cory, D. Candela, R.W. Mair, R. L. Walsworth, Noninvasive measurements of gas exchange in a three dimensional fluidized bed by hyperpolarized129Xe NMR, Appl. Magn. Reson. 32 (2007) 93–112.
[20] W. Wu, P.K. Agarwal, The effect of bed temperature on mass transfer between the bubble and emulsion phases in a fluidized bed, Can. J. Chem. Eng. 81 (2003) 940–948.
[21] M. Horio, C.Y. Wen, An assessment of fluidized-bed modelling, in: Fluid. Theor. Appl., American Institute of Chemical Engineers, New York, 1977, pp. 9–21.
[22] K. Kato, C.Y. Wen, Bubble assemblage model for fluidized bed catalytic reactors, Chem. Eng. Sci. 24 (1969) 1351–1369.
[23] J.J. van Deemter, Mixing and contacting in gas-solid fluidized beds, Chem. Eng. Sci. 13 (1961) 143–154.
[24] D. Kunii, O. Levenspiel, Bubbling bed model, Ind. Eng. Chem. Fundam. 7 (1968) 446–452.
[25] T. Chiba, H. Kobayashi, Gas exchange between the bubble and emulsion phases in gas-solid fluidized beds, Chem. Eng. Sci. 25 (1970) 1375–1385.
[26] H. Xie, Z. Sun, Mass transfer between bubbles and the dense phase in gas fluidized beds, Particuology 16 (2014) 213–217.
[27] F. Hernandez-Jimenez, A. Gomez-Garcia, D. Santana, A. Acosta-Iborra, Gas interchange between bubble and emulsion phases in a 2D fluidized bed as revealed by two-fluid model simulations, Chem. Eng. J. 215–216 (2013) 479–490.
[28] R. Clift, J.R. Grace, Continuous bubbling and slugging, in: Fluidization Second Ed., 1985, pp. 73–132.
[29] S.U. Sane, H.W. Haynes Jr., P.K. Agarwal, An experimental and modelling investigation of gas mixing in bubbling fluidized beds, Chem. Eng. Sci. 51 (1996) 1133–1147.
[30] T.Y.N. Dang, T. Kolkman, F. Gallucci, M. van Sint Annaland, Development of a novel infrared technique for instantaneous, whole-field, non invasive gas concentration measurements in gas–solid fluidized beds, Chem. Eng. J. 219 (2013) 545–557.
[31] J.A. Medrano, N.C.A. de Nooijer, F. Gallucci, M. van Sint Annaland, Advancement of an infra-red technique for whole-field concentration measurements in fluidized beds, Sensors (Switzerland) 16 (2016).
[32] C. Chavarie, J.R. Grace, Interphase mass transfer in a gas fluidized bed, Chem. Eng. Sci. 31 (1976) 741–749.
[33] R. Toei, R. Matsuno, H. Miyawaga, K. Nishitani, Y. Komawaga, Gas transfer between a bubble and the continuous phase in a gas-solid fluidized bed, Int. Chem. Eng. 9 (1969) 358–364.
[34] P.N. Rowe, T.J. Evans, J.C. Middleton, Transfer of gas between bubbles and dense phase in a two-dimensional fluidised bed, Chem. Eng. Sci. 26 (1971) 1943–1948.
[35] J. Gascon, C. Tellez, J. Herguido, H.A. Jakobsen, M. Menendez, Modeling of fluidized bed reactors with two reaction zones, AIChE J. 52 (2006) 3911–3923.
[36] F. Gallucci, M. van Sint Annaland, J.A.M. Kuipers, Autothermal reforming of methane with integrated CO_2 capture in a novel fluidized bed membrane reactor. Part 2 comparison of reactor configurations, Top. Catal. 51 (2008) 146–157.
[37] I. Iliuta, R. Tahoces, G.S. Patience, S. Rifflart, F. Luck, Chemical-looping combustion process: kinetics and mathematical modeling, AIChE J. 56 (2010) 1063–1079.
[38] R.M. Davies, G.I. Taylor, The mechanics of large bubbles rising through extended liquids and through liquids in tubes, Proc. R. Soc. 200 (1950) 375.
[39] V. Spallina, D. Pandolfo, A. Battistella, M.C. Romano, M. Van Sint Annaland, F. Gallucci, Techno-economic assessment of membrane assisted fluidized bed reactors for pure H_2 production with CO_2 capture, Energy Convers. Manage. 120 (2016) 257–273.